LIMNOLOGY and OCEANOGRAPHY

ASLO

Limnol. Oceanogr. 69, 2024, 2881–2895

doi: 10.1002/lno.12716

Different elemental stoichiometries of Fe-limited *Trichodesmium* when grown under inorganic and organic phosphorus sources

Xuechao Wang, Thomas J. Browning,* Eric P. Achterberg, Martha Gledhill
GEOMAR Helmholtz Centre for Ocean Research Kiel, Kiel, Germany

Abstract

Trichodesmium spp. is a colonial diazotrophic cyanobacterium found in the oligotrophic (sub)tropical oceans, where its distribution is strongly regulated by the availability of phosphorus and iron. The bulk carbon : nitrogen : phosphorus elemental composition of phytoplankton has previously been shown to depart from classical "Redfield" values under nutrient-limitation conditions. We hypothesized that the abundance of intracellular metabolites and the extended Redfield ratios of *Trichodesmium*, including a range of trace elements, are variable in response to conditions of phosphorus and iron limitation that are found in the ocean. To test this, we grew *Trichodesmium* under trace metal–controlled conditions, where phosphorus was supplied as either dissolved inorganic phosphorus (DIP) or dissolved organic phosphorus (DOP) from iron depleted to elevated levels. We found that the steady-state extended Redfield ratios of *Trichodesmium* under the iron-depleted condition was $(C_{106}N_{15.82}P_{0.62})_{1000}Fe_{2.26}Zn_{2.37}Mn_{1.68}Cu_{0.68}Ni_{0.31}Mo_{0.42}Co_{0.03}$ for the DIP treatment where *Trichodesmium* was under iron limitation, and $(C_{106}N_{13.89}P_{0.49})_{1000}Fe_{3.38}Zn_{2.51}Mn_{0.97}Cu_{0.52}Ni_{0.42}Mo_{0.33}Co_{0.03}$ for the DOP treatment where *Trichodesmium* was under iron–phosphorus co-limitation. Mean steady-state cellular iron : carbon in the DIP treatment (iron limited) was only 50% of that in the control treatment, while zinc : carbon was elevated twofold. The average extended Redfield ratios following recovery from iron limitation was $(C_{106}N_{16.8}P_{0.7})_{1000}Fe_{4.41}Zn_{1.44}Mn_{1}Cu_{0.52}Ni_{0.19}Mo_{0.3}Co_{0.03}$ for the DIP and $(C_{106}N_{15.9}P_{0.73})_{1000}Fe_{7.36}Zn_{2.24}Mn_{1.08}Cu_{0.71}Ni_{0.63}Mo_{0.38}Co_{0.02}$ for the DOP treatment. No significant changes were observed in the carbon-normalized abundance of targeted metabolites produced by *Trichodesmium*, under the different treatments. These results suggest *Trichodesmium* employs different strategies to cope with iron/phosphorus limitation, which is reflected in its extended Redfield ratios.

The low availability of bioavailable nitrogen (N) in surface waters of the (sub)tropical oceans is generally considered the main limiting factor for phytoplankton growth (Falkowski 1997; Moore et al. 2013). Diazotrophs, N_2-fixing microbes, can supply new bioavailable N to such environments, thereby increasing productivity. *Trichodesmium* is a colonial diazotroph species inhabiting surface waters of the low-latitude oceans (Capone et al. 1997). Although recent genomic discoveries have highlighted the diversity of additional diazotrophs in the ocean (Zehr and Capone 2020), *Trichodesmium* is still recognized as a critical contributor (Carpenter and Capone 2008; Shao et al. 2023).

In low-latitude N-depleted ocean regions, the distribution of *Trichodesmium* is strongly regulated by the availability of iron (Fe; Mark Moore et al. 2009; Sohm et al. 2011; Snow et al. 2015). Furthermore, recent evidence suggests that *Trichodesmium* becomes more abundant with enhanced expression of nitrogenase genes and higher N_2-fixation rates when it is co-limited by Fe–phosphorus (P) compared to single limitation by Fe or P (Garcia et al. 2015; Walworth et al. 2016, 2018; Held et al. 2020; Cerdan-Garcia et al. 2021). An important part of the development of this co-limitation condition is thought to be the ability of *Trichodesmium* to access a broad range of dissolved organic P (DOP) compounds under conditions of low dissolved inorganic P (DIP), using enzymes including alkaline phosphatases and C–P lyases (Dyhrman et al. 2006; Orchard et al. 2010; Morrissey and Bowler 2012).

Previous studies have focused mainly on the availability of Fe and P in relation to the distribution, growth rate, N_2-fixation rate, alkaline phosphatase activity (APA), major

*Correspondence: tbrowning@geomar.de

Additional Supporting Information may be found in the online version of this article.

Author Contribution Statement: TB, MG, and XW designed the study. XW performed culture work, data collection, analysis, and wrote the manuscript. TB, EA, and MG contributed editorial comments and approved the final version of the manuscript. All authors contributed to the article and approved the submitted version.

elemental stoichiometry, transcriptomics, and proteomics of *Trichodesmium* (Chen et al. 1996; Hynes et al. 2009; Ho 2013; Yamaguchi et al. 2016; Tzubari et al. 2018; Frischkorn et al. 2019; Cerdan-Garcia et al. 2021). The stoichiometry of individual species and taxonomic groups can vary significantly (Ho et al. 2003; Twining et al. 2010), meanwhile the stoichiometry of the same species can vary depending on the ambient environmental conditions (Nuester et al. 2012). Phytoplankton elemental stoichiometry is known to be a key determinant of ocean biogeochemical cycling, regulating phytoplankton growth rates and elemental concentrations in the ocean (Moore et al. 2013). However, studies on the elemental stoichiometry of *Trichodesmium* under Fe- and/or P-limited conditions are relatively scarce (White et al. 2006; Nuester et al. 2012). Trace metals are essential cofactors for many of the enzymes involved in the acquisition and utilization of N and P, and include Fe and Mo for N_2-fixation (Dominic et al. 2000; Tuit et al. 2004), Zn and/or Fe in alkaline phosphatases (Kim and Wyckoff 1991; Rodriguez et al. 2014; Yong et al. 2014), Ni for hydrogenases and superoxide dismutase (Ho et al. 2013; Tuo et al. 2020), and Cu for reductive deamination of amines and amino acids and plastocyanin (Palenik and Morel 1991). Therefore, there is a complex set of linkages between the biological use of N, P, and trace metals in *Trichodesmium*. Determining how the elemental stoichiometry of *Trichodesmium* changes in response to changes in Fe- and P-limitation and under growth on different P sources is therefore critical for understanding, and ultimately, accurate modeling of N_2 fixation in the ocean.

Metabolomics is a powerful tool to explore the physiology and chemical ecology of marine organisms (Johnson et al. 2016; Durham et al. 2017; Kujawinski et al. 2017; Heal et al. 2019; Dawson et al. 2020; Johnson et al. 2023). Cell metabolism is highly plastic, responding to environmental conditions in marine phytoplankton under variable P-availability (Kujawinski et al. 2017). Moreover, the composition of metabolites in phytoplankton cells is regulated by their growth phase (Barofsky et al. 2009, 2010; Vidoudez and Pohnert 2012; Fiore et al. 2015; Mausz and Pohnert 2015). While the abundance of intracellular proteins, lipids, and nucleic acids in *Trichodesmium* have been demonstrated to be regulated by P- and Fe-limitation (Walworth et al. 2016; Kujawinski et al. 2017), metabolites such as some specific nucleic acids remain uninvestigated.

We tested for the impact of the relative availability of different P sources and Fe on cellular elemental quotas and particulate metabolites in *Trichodesmium* IMS101. Two P sources were utilized: (i) 5 μM DIP and (ii) 5 μM methylphosphonic acid (MPA), a phosphonate synthesized by marine microbes (Metcalf et al. 2012), and phosphonates make up to 25% of the DOP pool (Clark et al. 1999; Sannigrahi et al. 2006). Experiments were conducted in large volumes (2 liters) with triplicate replication using an exponentially fed batch culture approach (Fischer et al. 2014; Marki et al. 2020), which allows for regular harvesting of sufficient biomass required for bulk phytoplankton elemental and metabolite analyses.

Materials and methods

Cultures

To examine effects of different Fe concentrations on growth of the diazotrophic cyanobacterium *Trichodesmium* IMS101, *Trichodesmium* was purchased from NCMA (https://ncma.bigelow.org/), it was cultured with 5 μM DIP and 5 μM MPA separately in triplicate under supply of Fe-depleted media (4 nM; 33 d) and then Fe replete media (40 nM; 21 d) using an exponentially fed batch culture system (Fischer et al. 2014; Marki et al. 2020; Supporting Information Fig. S1). With the exponentially fed batch, the amount of media added is proportional to the culture volume, so the supply rate of the media increases exponentially over time to establish a constant dilution rate. We followed the culture method throughout the study as described by Marki et al. (2020). All manipulations of media and samples were performed in a laminar flow hood fitted with a high-efficiency particulate air filter. All materials were acid-soaked in 1.2 M HCl for more than 1 week and rinsed with ultrapure water (MilliQ; ≤ 18 MΩ cm^{-1}; Millipore) prior to use, with the exception of sterile culture bottles, which were used as supplied by the manufacturer. In a control treatment *Trichodesmium* was cultured with a constant media supply of 5 μM DIP and 40 nM Fe where Fe was added as a complex with EDTA. The cultures were maintained in the exponentially fed batch cultures at 25°C on a 12 h/12 h light/dark cycle at 140 μmol photons m^{-2} s^{-1} in YBCII media (Chen et al. 1996). The YBCII media was prepared with ultrapure water and analytical reagent grade salts (Supporting Information Table S1). Reagents were not passed through a cation exchange resin. The YBCII media was adjusted to pH 7.8–8.1 by addition of 0.01 M sodium hydroxide and filter sterilized with disposable rapid flow filter units (polyethersulfone 0.1 μm, Nalgene). Ten liters of high-density polyethylene carboys (Nalgene) were used as YBCII culture media reservoirs. Cultures were grown in sterile polycarbonate culture bottles (2 liters, Nalgene). The initial volume of the cultures was 1400 mL into which fresh media was pumped using narrow bore polypropylene tubing (inner diameter 0.51 mm, Ismaprene, Pharmed) with a peristaltic pump (IPC-N, Ismatec) via a filter (0.2 μm; Sterivex). Before use, continuous injection of 1.2 M HCl was carried out into the narrow bore polypropylene tubing using a peristaltic pump for 30 min; subsequently, a 30-min injection of deionized water was performed to complete the cleaning process. The peristaltic pump was controlled by a programmable microcontroller (Raspberry Pi 3), which automatically increased the flow rate each hour in relation to the real-time culture volume, thereby maintaining a constant culture dilution rate of 0.1 d^{-1}. The dilution rate employed together with the starting volume allowed a single time point recovery of $\sim$ 500 mL of sample every 3 d. All

sample collection and media preparation were carried out in a laminar flow hood equipped with a high efficiency particulate air filter, located within a trace metal clean laboratory. To ensure sample consistency throughout the experiment and minimize potential impacts on *Trichodesmium* stoichiometry and metabolite concentrations due to varying sampling times, all samples were collected at 9:00 a.m., precisely 1 h after the initiation of the light cycle.

Before commencing the experiments, *Trichidesmium* were cultured with 5 μM DIP in a set of six replicates and 5 μM MPA in triplicate under supply of 40 nM Fe for 10 d. Immediately after the 10 d there was no significant difference (Quade post hoc test; $p < 0.05$) in POC over time; at $T = 0$, the supply of Fe was subsequently reduced to 4 nM in the DIP and DOP groups; at $T = 33$, the supply of Fe was subsequently induced to 40 nM in the DIP and DOP groups.

Fast repetition rate fluorometry

Fast repetition rate fluorometry of *Trichodesmium* cultures was conducted throughout the whole culture period with a FASTOcean sensor equipped with a FASTAct laboratory system (Chelsea Technologies Group). Samples were dark acclimated for 30 min in the culture cabinet prior to measurements (Trimborn et al. 2017; van de Poll et al. 2020). Recovery of minimum fluorescence (F_0) and maximum fluorescence (F_m) using FASTPro8 software (Chelsea Technologies Group) allowed determination of the potential photochemical efficiency of photosystem II (PSII; $F_v/F_m = (F_m - F_o)/F_m$). The ratio of variable fluorescence to maximum fluorescence (F_v/F_m) has a variety of controls including phytoplankton species, light climate, and nutrient limitation (Suggett et al. 2009). However, under conditions of a single phytoplankton species growing under the same light conditions, differences in nutrient limitation is the major driver of variability (Suggett et al. 2009; Behrenfeld and Milligan 2013). More specifically, under conditions of steady-state nutrient limitation—as used in this study—the relative levels of Fe-limitation have the strongest impact on F_v/F_m, with elevated values under no Fe-limitation (with or without prevalent macronutrient limitation) and strongly decreased values under Fe-limited conditions (Behrenfeld and Milligan 2013).

Alkaline phosphatase activity

Whole water APA rates were measured using the fluorometric substrate 4-methylumbelliferyl phosphate (Sigma-Aldrich) following the protocol of Ammerman (1993). Concentrated (100 mM) 4-methylumbelliferyl phosphate and 4-methylumbelliferone (Sigma-Aldrich) stock solution was prepared by dissolving 4-methylumbelliferyl phosphate and 4-methylumbelliferone into 2-methoxyethanol. Working stocks (100 μM) were made daily by diluting this concentrated stock with ultrapure water. The assays were started by adding 100 μL of 4-methylumbelliferyl phosphate to 5 mL samples in replicate 15-mL tubes to yield a final substrate concentration of 2 μM. A 150 μL subsample was transferred into a 96-well plate immediately from the mixed sample. Then, 50 μL of filtered 50 mM borate buffer (pH 10.8) was added to the subsample in the well plate and mixed to a final pH > 10. Alkaline phosphatase activity was measured on a temperature-controlled (25°C) plate reader (FLX800TBI, BioTek) with Gen 5 software using an excitation wavelength of 365 nm and an emission wavelength of 455 nm. Fluorescence measurements were performed at $t = 0$, 1, and 2 h. Alkaline phosphatase activity (h^{-1}) was calculated as the fluorescence of a 2 μM 4-methylumbelliferone divided by the initial ($t = 0$–2 h) slope of fluorescence time course (fluorescence per hour). Regular ultrapure blanks and paraformaldehyde-killed controls were conducted and generally yielded fluorescence values similar to $t = 0$ readings.

Nutrients

Samples of dissolved inorganic nitrate + nitrite and P (15 mL) were filtered through glass fiber filters (25 mm, 0.7 μm, Fisherbrand) under low pressure (200 MPa). Samples were stored in polypropylene tubes (15 mL, Fisherbrand) at –20°C until analysis and then analyzed using a SEAL QuAAtro nutrient autoanalyzer system (SEAL Analytical; Becker et al. 2020). Detection limits for the nutrient analyses, calculated as three times the standard deviation of a blank measured during the analytical run, were nitrate + nitrite = 0.06 μmol L^{-1}; phosphate = 0.02 μmol L^{-1}. Samples of total dissolved P (TDP; 50 mL) were filtered through sterile polyethersulfone syringe filters (0.2 μm, Fisherbrand). Samples were stored in polypropylene tubes (50 mL, Fisherbrand) at −20°C. Prior to analysis, total dissolved P samples and blanks were digested under elevated pressure (1.5 bar) and temperature (120°C) for 30 min following addition of the oxidizing reagent Oxisolv (Merck), and then analyzed using a SEAL QuAAtro nutrient autoanalyzer system (SEAL Analytical). Dissolved organic phosphorus concentration was subsequently calculated as DOP = total dissolved P − DIP.

Particulate organic C/N

Particulate organic C/N concentrations were determined by filtering 50 mL sample through pre-combusted (500°C, 12 h) glass fiber filters (25 mm, 0.7 μm, Fisherbrand) under low pressure (200 MPa). Filters were stored frozen at −20°C. Prior to analysis, filters were dried at 50°C for 12 h. After drying, filters were wrapped in tin boats (8 × 8 × 15 mm) and put in a well plate and stored in desiccator. Samples and blanks were analyzed using an elemental analyzer (Eurovector EA3000 Elemental Analyzer) with Callidus version 5.1 software.

Particulate element concentration

Fifty milliliters of sample were filtered on to acid-cleaned (10% HCl) polyethersulfone membrane filters (25 mm, 0.8 μm, PALL). Filters were frozen and stored at −20°C until digestion. Cell digestion following the method described by Honey et al. (2013) and Marki et al. (2020), filters were placed in acid-washed (20% HNO_3) 15-mL PFA digestion vials with

2 mL of concentrated redistilled HNO_3 (Savillex, QMX) and heated to 120°C for 24 h (Al-Hashem et al. 2022). The filter was removed from the vial and the HNO_3 evaporated off (75°C, overnight). The residue was dissolved in 3 mL of 1% HNO_3 and spiked with indium (4 μg L^{-1}) as an internal standard. The samples were then centrifuged at 14,000 rpm (Centrifuge 5430R, Eppendorf) for 10 min, and the upper supernatant was taken for determination by inductively coupled plasma mass spectrometry (Element XR, Thermo Fisher), using prepared elemental standard calibrations for quantification. Table 1 contains details on program blank values and detection limits.

Metabolite concentrations

Targeted metabolites and their basic function are listed in Supporting Information Table S2. A 250 mL sample was transferred to a bioprocessing bag (Standard Flexboy, 500 mL). Before filtration, 250 μL optima-grade formic acid together with 25 μL internal standard (860 μg L^{-1} D6 biotin, 630 μg L^{-1} $C_{13}N_{15}$ Riboflavin) was added to the 250 mL of sample. A filter unit (Sterivex PVDF, 0.2 μm, Millipore) was connected to the bioprocessing bag via a PharMed BPT tubing (PharMed, 1 m). The bioprocessing bag was then suspended 2 m above the ground at room temperature to complete the filtration using gravity (3–5 h). Filters were frozen and stored at −80°C until elution. For sample elution, 2 mL of cold (−20°C) extraction solvent (40 : 40 : 20 acetonitrile : methanol : 0.1 M formic acid v : v : v) was added to each filter unit to cover the filter pieces. The filter units were capped and ultra-sonicated on ice for 20 min. After ultra-sonication, the extracted metabolites were collected into a 2-mL pre-weighed Eppendorf vial, vials were placed in centrifugal evaporator and the solvents evaporated overnight. The weight of the sample after evaporation ranged from 0.1 to 0.4 g. A 50 μL sample was transferred to a high-performance liquid chromatography vial and spiked with 5 μL yeast extract containing ^{13}C-labeled metabolites (U-13C, Cambridge Isotope Laboratories, 98%). Additional samples for quality control were analyzed in all experiments (Kido Soule et al. 2015). These quality control samples consisted of a mixed standard of authentic metabolites and a pooled sample consisting of aliquots of each sample (50 μL). Metabolites were separated by reversed-phase high-performance liquid chromatography (Synergi Fusion 4 μm, 2 × 150 mm) and detected by electrospray ionization mass spectrometry (Thermo Fisher Q-Exactive). Solvents were (A) 10 mM ammonium formate : 5% methanol and (B) methanol. Metabolites were separated using a delayed linear gradient elution that started at 100% A, ramped from 100% to 50% A at 9 min and then to 100% B at 12 min. Elution of metabolites was followed by a column wash with 100% B (2 min), and then a return to starting conditions and a 4-min column equilibration prior to injection of the next sample. Peak areas and retention times for known metabolites were processed in mzmine (https://mzmine.github.io/) using a targeted feature detection approach. The concentrations of ^{13}C-labeled metabolites in the yeast extract were quantified for each sample batch with unlabeled standards, and this concentration was then used to determine the concentration of each metabolite in the sample from the ratio of the isotopes. For compounds lacking unlabeled standards, we used the ^{13}C-labeled metabolite to normalize the response across all the samples.

Table 1. Values for procedural blanks and detection limit. The limit of detection is defined as three standard deviations of the procedural blank. All values in pM.

Analyte	Procedural blank	Detection limit (3 × SD)
Fe	72 ± 17	52
Zn	94 ± 22	66
Mn	15 ± 4	13
Cu	14 ± 4	12
Ni	122 ± 51	154
Mo	7 ± 2	6
Co	2.7 ± 0.7	2

Results and discussion

Trichodesmium responses to Fe-availability

Trichodesmium carbon biomass under the Fe-depleted condition decreased to 0.55 and 0.61 times the initial values within 24 d in the DIP and DOP treatments, respectively, after which no significant changes were observed (Quade post hoc test; $p < 0.05$; Fig. 1a; Supporting Information Fig. S2i,ii). At this point (days 24–33) we assumed that growth had reached an approximate steady state matching the dilution rate of the culture (0.1 d^{-1}). The biomass concentration at this point is dictated by the concentration of the most limiting nutrient in the culture media (Fischer et al. 2014), which in the case of the Fe-depletion experiment was Fe (DIP treatment), or both Fe and bioavailable P (DOP treatment; *see* "Discussion"). After restoring the Fe concentration in the media reservoir to 40 nM on day 33, *Trichodesmium* biomass within both treatments increased gradually to 1.9- and 1.02-fold of the steady-state Fe-limited values, respectively (Fig. 1a; Supporting Information Fig. S3a). After day 42 (DIP) and day 48 (DOP), no significant biomass changes were observed, and *Trichodesmium* was assumed to have recovered from Fe-limitation (Quade post hoc test; $p < 0.05$; Fig. 1a). The *Trichodesmium* recovery time from the Fe-depletion was therefore 9 and 15 d for DIP and DOP, respectively (Fig. 1a).

The nutrient limitation status of each treatment through the Fe-depletion and Fe-recovery phases could be dissected via observed changes in DIP concentrations, APA, and F_v/F_m (Fig. 1b,d,e). At time $t = 0$, *Trichodesmium* in both the DIP and DOP treatments was assumed to be under P-limitation, with both treatments having fully depleted DIP concentrations (< 0.1 μM; Fig. 1b). Carbon-normalized APA was however elevated 2.5-fold in the DOP treatment over the DIP treatment

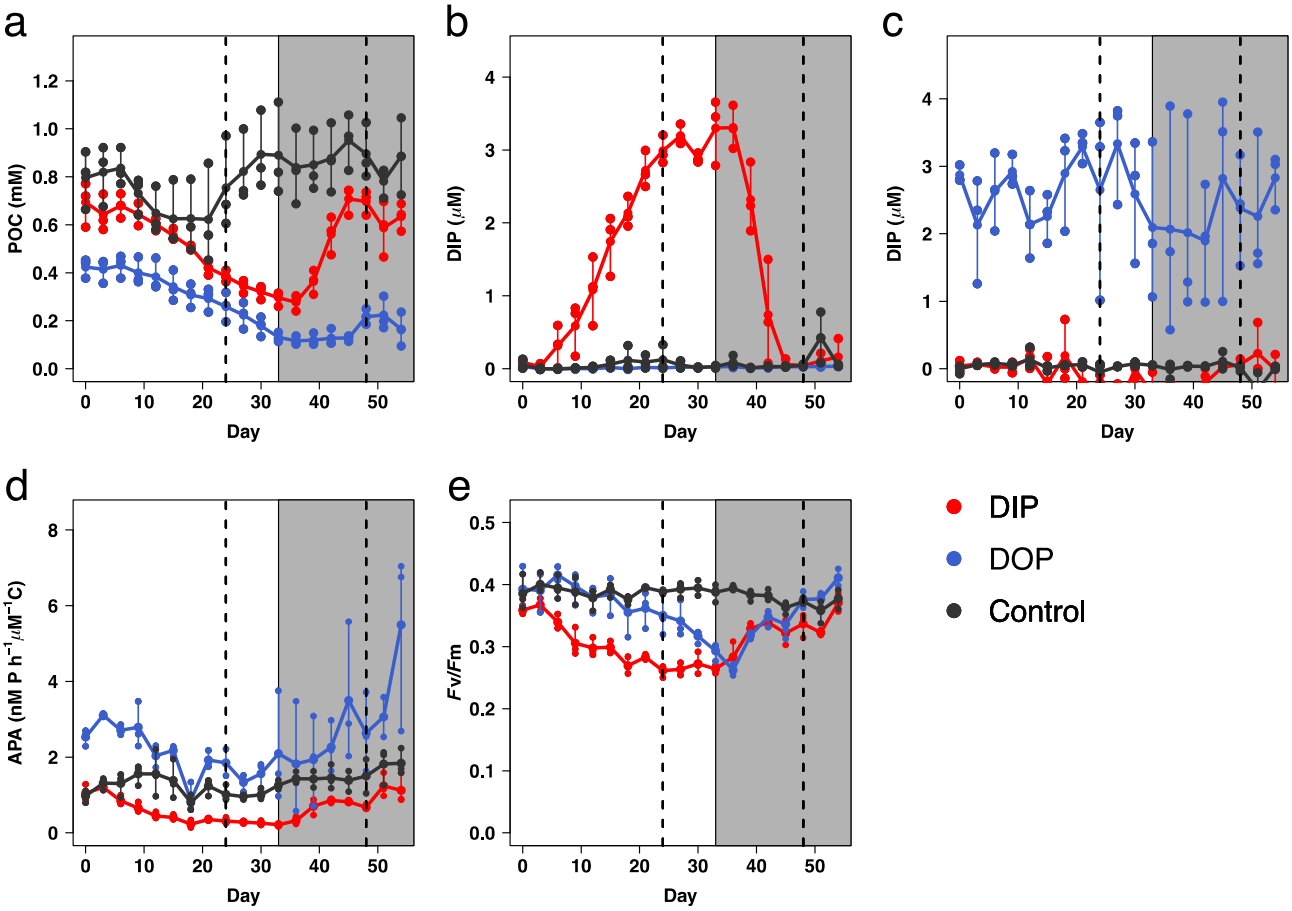

Fig 1. Responses of *Trichodesmium* IMS 101 under DIP and DOP phosphorus sources to variations in Fe supply. (**a**) POC concentration over time for the three treatments. (**b**) DIP concentration over time for the three treatments. (**c**) DOP concentration over time for the three treatments. (**d**) POC-normalized APA over time for the three treatments. (**e**) *Fv*/*Fm* values over time for the three treatments. Points show triplicate measurements from the biologically independent replicates every 3 d, lines map the change in the mean value with time. The left part without shading indicates period where Fe-depleted (4 nM) media was supplied. The shaded region indicates where the high Fe (40 nM) media was supplied. The time period to the right side of the dashed line for each condition is considered here to be at steady state (Quade post hoc test; $p < 0.05$).

(Fig. 1d), suggesting this treatment was under stronger P-limitation than the DIP treatment, consistent with a lower availability of this P source (Duhamel et al. 2010; Mahaffey et al. 2014). In addition, F_v/F_m values in the DIP treatment were lower than the control or DOP treatments (0.36; Fig. 1e), suggesting that the DIP treatment was potentially under co-limitation by DIP and Fe, as previously found under steady state when supplying this media to *Trichodesmium* (Wang et al. 2022). Application of the Fe-depleted media led to a steady rise in DIP concentrations for the DIP treatment, reaching to 3.09 ± 0.28 μM at steady state (day 24; Fig. 1b). This DIP increase was accompanied by a 0.75-fold decrease in APA (Fig. 1d) and a 0.27-fold decrease in F_v/F_m (Fig. 1e), both further pointing toward a shift from P-limitation, or P–Fe co-limitation, into stronger Fe-limitation (Schrader et al. 2011; Mahaffey et al. 2014). The DOP treatment contrasted with the DIP treatment upon application of the Fe-depleted media in showing no DIP accumulation, a more gradual F_v/F_m reduction, and APA levels that remained elevated. Together this demonstrated that this treatment was shifting from strong P-limitation through to Fe–P co-limitation.

During the Fe-recovery phase (after restoring the reservoir Fe concentration back to 40 nM), *Trichodesmium* in both DIP and DOP treatments started to revert back to the original conditions: DIP remained depleted in the DOP treatment but decreased steadily in the DIP treatment to full depletion by day 48 (0.06 ± 0.07 μM; Fig. 1b); APA increased in both but was 3.7-fold lower in the DIP treatment at steady state (Fig. 1d), and F_v/F_m increased in both treatments, but to a lower value in the DIP treatment (Fig. 1e). Together these indicated a return to P-limitation in the DOP treatment and a situation of P–Fe co-limitation in the DIP treatment.

Elemental stoichiometry

The overall average, steady-state elemental stoichiometry of *Trichodesmium* under the Fe-depleted condition

was $(C_{106}N_{15.82}P_{0.62})_{1000}Fe_{2.26}Zn_{2.37}Mn_{1.68}Cu_{0.68}Ni_{0.31}Mo_{0.42}Co_{0.03}$ for the DIP treatment and $(C_{106}N_{13.89}P_{0.49})_{1000}Fe_{3.38}Zn_{2.51}Mn_{0.97}Cu_{0.52}Ni_{0.42}Mo_{0.33}Co_{0.03}$ for the DOP treatment (Fig. 2a). The average elemental stoichiometry following Fe recovery was $(C_{106}N_{16.8}P_{0.7})_{1000}Fe_{4.41}Zn_{1.44}Mn_{1}Cu_{0.52}Ni_{0.19}Mo_{0.3}Co_{0.03}$ for the DIP treatment and $(C_{106}N_{15.9}P_{0.73})_{1000}Fe_{7.36}Zn_{2.24}Mn_{1.08}Cu_{0.71}Ni_{0.63}Mo_{0.38}Co_{0.02}$ for the DOP treatment (Fig. 2b).

The mean steady-state N : C ratio under the Fe-depleted condition for both the DIP and DOP treatments was significantly lower than that in the control treatment (0.149 ± 0.024, 0.131 ± 0.010 and 0.157 ± 0.008 mol mol^{-1} for DIP, DOP, and control treatments, respectively; Fig. 2a; Table 2). Which is similar to the N : C ratio of the *Trichodesmium* colonies collected from the Sargasso Sea measured by Nuester et al. (2012), the N : C ratios were from 0.147 to 0.178 mol mol^{-1}. Declining N : C ratios under Fe-limitation were consistent with previous studies (Beversdorf et al. 2010). The nitrogenase complex of *Trichodesmium* has been predicted

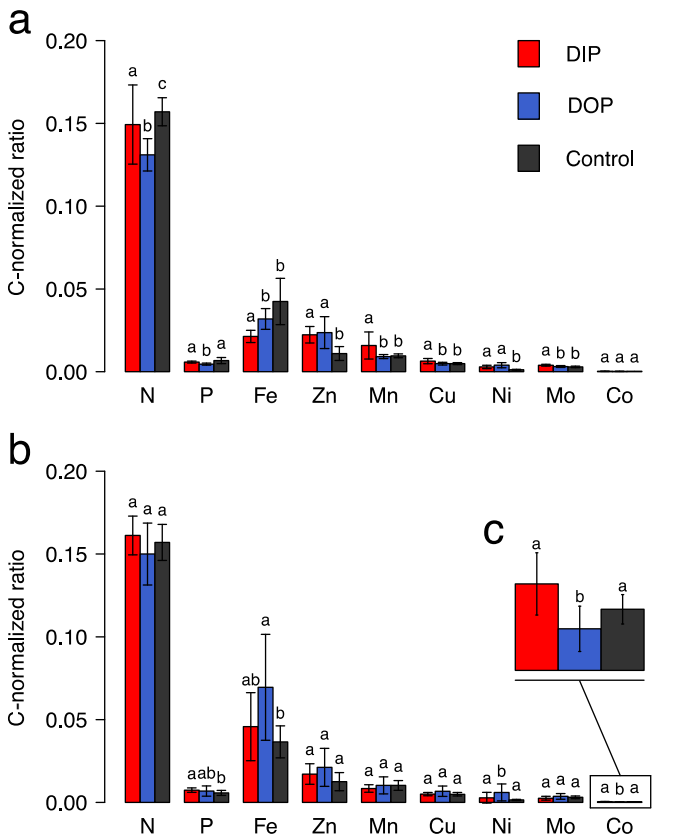

Fig 2. Elemental composition of *Trichodesmium* IMS 101 at steady state for (**a**) Fe-depleted media (4 nM), (**b**) Fe-replete media (40 nM), and (**c**), bar plot of C-normalized Co ratio. Bars show the mean steady-state elemental ratios, error bars are the standard deviation ($n = 7$–12 biologically independent replicates). N and P are in units of mol : mol; all others are in units of mmol : mol. Bars labeled with the same letter have means that are statistically indistinguishable between treatments with the applied statistical test (pairwise Wilcox test, $p < 0.05$).

Table 2. Mean steady-state carbon-normalized elemental ratios of *Trichodesmium* IMS101 under Fe-depleted (upper) and Fe-recovery (bottom area with shading) conditions. Standard deviations are shown in the smaller font ($n = 3$ biologically independent replicates).

Treatment	N (mol mol^{-1})	P (mol mol^{-1})	Fe (mmol mol^{-1})	Zn (mmol mol^{-1})	Mn (mmol mol^{-1})	Cu (mmol mol^{-1})	Ni (mmol mol^{-1})	Mo (mmol mol^{-1})	Co (mmol mol^{-1})
DIP	0.1490	0.0058	0.0213	0.0220	0.0158	0.0064	0.0029	0.0039	0.0003
	0.0240	0.0006	0.0037	0.0050	0.0082	0.0016	0.0010	0.0006	0.0001
DOP	0.1310	0.0046	0.0319	0.0240	0.0092	0.0049	0.0039	0.0031	0.0003
	0.0100	0.0006	0.0060	0.0100	0.0012	0.0008	0.0016	0.0005	0.0000
Control	0.1570	0.0068	0.0424	0.0110	0.0096	0.0049	0.0012	0.0030	0.0003
	0.0080	0.0018	0.0013	0.0040	0.0012	0.0006	0.0003	0.0005	0.0001
DIP	0.1610	0.0073	0.0457	0.0171	0.0084	0.0050	0.0028	0.0025	0.0004
	0.0120	0.0013	0.0206	0.0062	0.0023	0.0010	0.0032	0.0012	0.0002
DOP	0.1500	0.0068	0.0695	0.0211	0.0103	0.0067	0.0060	0.0037	0.0002
	0.0190	0.0031	0.0320	0.0115	0.0051	0.0031	0.0051	0.0017	0.0001
Control	0.1570	0.0057	0.0366	0.0125	0.0103	0.0049	0.0014	0.0031	0.0003
	0.0110	0.0015	0.0097	0.0055	0.0029	0.0010	0.0003	0.0008	0.0001

to host 19–53% of cellular Fe (Kustka et al. 2004), with the abundance of nitrogenase and rates of N_2 fixation reducing under Fe-limitation (Shi et al. 2007; Snow et al. 2015). Therefore, we suggest that lowered Fe-availability limited N_2 fixation, in turn reducing N : C quotas. Under Fe recovery, the N : C ratio increased for both the treatments, and at steady state no significant differences in N : C ratios from the control treatment were observed (0.161 ± 0.012, 0.15 ± 0.019, and 0.157 ± 0.011 mol mol^{-1} for DIP, DOP, and control treatments, respectively; Fig. 2b; Table 2).

No significant differences were observed between the mean steady-state P : C ratio in the DIP and control treatments under the Fe-depleted condition, but both were significantly higher than in the DOP treatment ($[5.8 \pm 0.6] \times 10^{-3}$, $[4.6 \pm 0.6] \times 10^{-3}$, and $[6.8 \pm 1.8] \times 10^{-3}$ mol mol^{-1} in DIP, DOP, and control treatments, respectively; Fig. 2a; Table 2). This is consistent with the expectation of lowest P-availability in the DOP treatment under this condition (Fig. 1b,c). Interestingly, *Trichodesmium* in both the DIP and DOP treatments increased their P : C ratio upon Fe-recovery (1.26- and 1.48-fold, respectively). This occurred despite a situation of strengthening P-limitation (Fig. 1b,d), but the values were consistent with our previous work (Wang et al. 2022).

Iron quotas for both DIP and DOP treatments decreased in response to reduced Fe-availability, consistent with previous findings (Kustka et al. 2004; Berman-Frank et al. 2007; Nuester et al. 2012; Shi et al. 2012), but showed subtle differences depending on the degree of Fe-limitation (Fig. 2a; Table 2). Specifically, under the steady-state Fe-depleted condition, the DIP treatment was under strongest Fe-limitation and had the lowest Fe : C ratio (0.0213 ± 0.0037 mmol : mol), the control treatment was under no Fe-limitation and it had the highest Fe : C ratio (0.0424 ± 0.0013 mmol : mol), while the DOP treatment was under probable Fe–P co-limitation and had an intermediate Fe : C ratio (0.0319 ± 0.0062 mmol : mol). Our data are similar to the Fe : C ratio of the *Trichodesmium* colonies collected from the Sargasso Sea measured by Nuester et al. (2012), which were from 21 to 40 μmol mol^{-1}. The 1.5 times higher Fe : C ratios in the DOP treatment compared to the DIP treatment under the steady state, Fe-depleted condition, could be a consequence of weaker Fe-limitation due to co-limitation by P as well as Fe; however, enhanced cellular Fe quotas under lower P-availability could also play a role. Specifically, although MPA cannot be hydrolyzed by alkaline phosphatase, mean steady-state APA in the DOP treatment was roughly 8.5-fold of that in DIP treatment (Fig. 1d), suggesting much higher production of AP enzymes which include the Fe-containing forms PhoX and PhoD (Luo et al. 2011). In addition, MPA is utilized by *Trichodesmium* via C–P lyases, which also contain Fe (Stosiek et al. 2020). Upon Fe recovery, steady-state Fe : C ratios in the DIP and DOP treatments increased 2.14- and 1.69-fold over the Fe-depleted condition, respectively (Fig. 2b, Table 2), reaching to $(7.3 \pm 1.3) \times 10^{-3}$ and $(6.8 \pm 3.1) \times 10^{-3}$ mol mol^{-1}, respectively, consistent with increased Fe-availability in both treatments, which were $(7.1 \pm 1.4) \times 10^{-3}$ and $(7.2 \pm 2.5) \times 10^{-3}$ mol mol^{-1}.

No significant differences were observed between mean steady-state Zn : C ratio in the DIP and DOP treatments under the Fe-depleted condition, while both of them were significantly higher than in the control treatments (0.022 ± 0.005, 0.0024 ± 0.01, and 0.011 ± 0.004 mmol : mol in the DIP, DOP, and control treatments, respectively; Fig. 2a; Table 2). In the steady-state Fe-recovery-phase Zn quotas showed decreases in both DIP and DOP treatments. This contrasts with previous work (Wang et al. 2022) that showed 3.5-fold increases in Zn quotas under strong P-limitation under growth on MPA in comparison to DIP. However, closer inspection of the Fe-recovery phase showed Zn quotas in the DOP treatment increased 3.1-fold over 6 d, but then decreased moving into steady state (Fig. 3d), suggesting that Zn accumulation under P-limitation could be time scale dependent.

The quotas of several other trace elements increased under strongest Fe-limitation found in the DIP treatment in the Fe-depletion phase : mean steady-state ratios of Mn : C, Cu : C, and Mo : C in were significantly higher (1.65-, 1.31-, and 1.3-fold) than that in the control treatment (Quade post hoc test; $p < 0.05$; Fig. 2a; Table 2). These decreased in the Fe recovery phase (Fig. 2b; Table 2). The absolute requirement for Mn in photosynthesis is well known (Raven et al. 1999) with increased requirements for Mn under low Fe-availability reported for diverse phytoplankton including cyanobacteria as well as diatoms, likely due to a substitutable Fe or Mn requirement for superoxide dismutase enzymes (Peers and Price 2004; Salomon and Keren 2011, 2015; Sharon et al. 2014; Kaushik et al. 2015; Marki et al. 2020). Enhanced Cu requirements under stronger Fe-limitation could potentially be ascribed to the substitution of Fe-containing cytochrome c_6 with Cu-containing plastocyanin within the photosynthetic electron transport chain (Peers et al. 2005; Peers and Price 2006; Schoffman et al. 2016). The mechanism leading to enhanced Mo quotas is more difficult to ascribe, although its requirement in nitrogenase alongside Fe could conceivably lead to enhanced assimilation into different forms of nitrogenase or enhanced uptake due to reduced competition for Fe uptake sites at low Fe concentrations (Pau 2004; Hernandez et al. 2009).

No significant differences were observed between the mean steady-state Ni : C ratios in the DIP and DOP treatments under the Fe-depleted condition, while both of them were significantly higher than in the control treatment (0.0029 ± 0.0010, 0.0039 ± 0.0016, and 0.0012 ± 0.0003 mmol : mol in the DIP, DOP, and control treatments, respectively; Figs. 2a, 3i; Table 2). In the steady-state Fe-recovery phase, Ni quotas showed increases in DOP treatment with the mean steady-state Ni : C ratio for DOP treatment significantly higher than in the DIP and control treatments (0.0028 ± 0.0032, 0.0060 ± 0.0051, 0.0014 ± 0.0003 mmol : mol in the DIP,

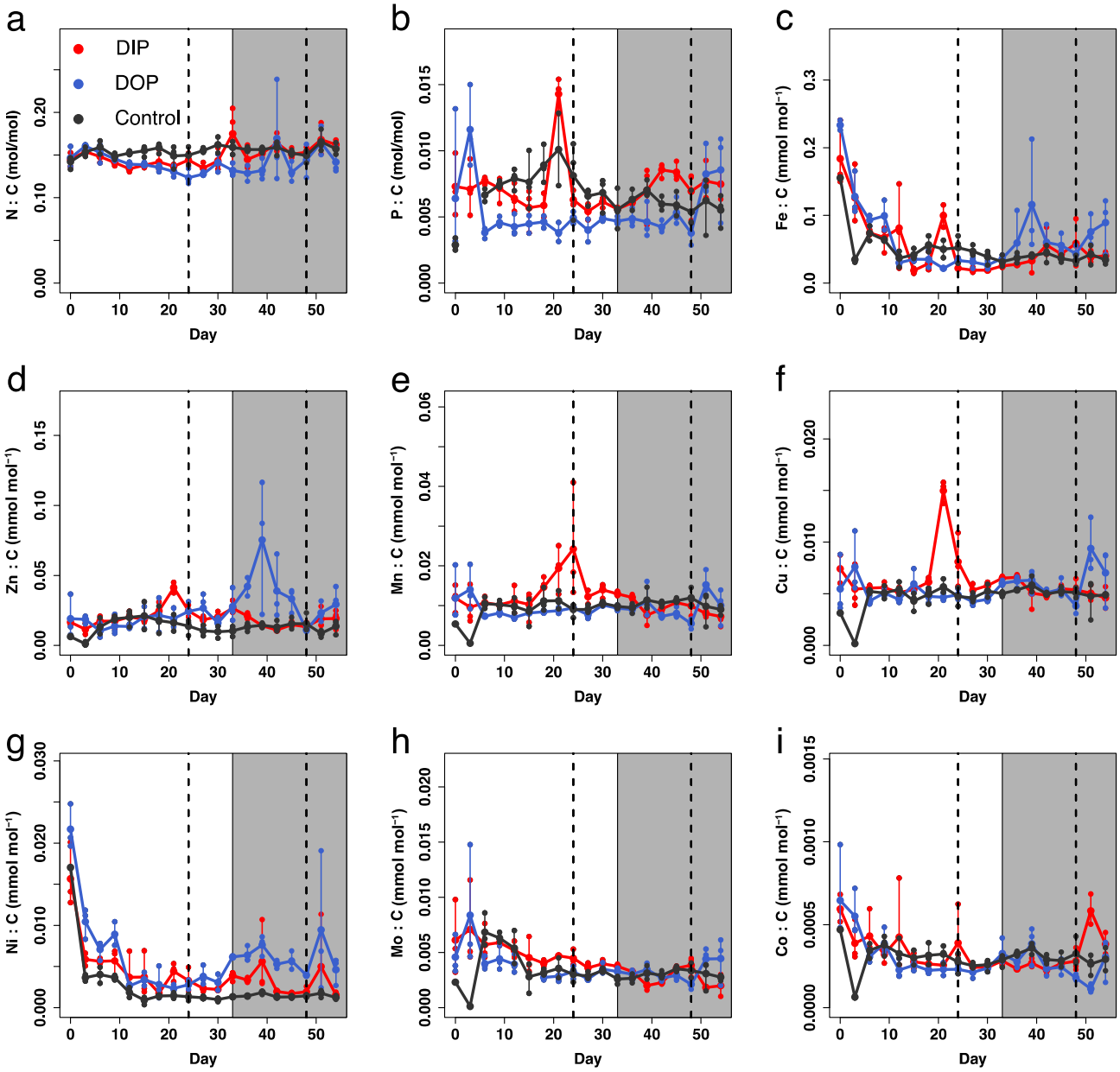

Fig 3. Elemental responses of *Trichodesmium* IMS 101 under DIP and DOP phosphorus sources to variations in Fe supply. (**a–j**) N : C, P : C, Fe : C, Zn : C, Mn : C, Cu : C, Ni : C, Mo : C, and Co : C ratios over time for the three treatments. Points show triplicate measurements every 3 d, lines map the change in the mean value with time. The left part without shading indicates the period where Fe-depleted (4 nM) media was supplied. The shaded region indicates where the high Fe (40 nM) media was supplied. The time period to the right side of the dashed line for each condition is considered here to be at steady state (Quade post hoc test; $p < 0.05$).

DOP, and control treatments, respectively; Figs. 2a, 3i; Table 2). Nickel is essential for the growth of *Trichodesmium* and increased requirement for Ni in cyanobacteria grown under P-limitation has previously been reported (Ji and Sherrell 2008). Phosphorus limitation of cyanobacteria can result in the production of reactive oxygen species (Wu et al. 2012) and to avoid potential reactive oxygen species–derived damage, *Trichodesmium* produce superoxide dismutase, some forms of which require Ni (Puppo and Rigaud 1986; Ho 2013; Ho et al. 2013). This suggests that enhanced Ni requirements under stronger P-limitation could potentially be a result of increased activity of Ni-requiring superoxide dismutase under P-limitation (Ji and Sherrell 2008; Ho et al. 2013; Chen et al. 2022). No significant differences were observed among mean steady-state Co : C ratios in all the treatments under the Fe-depleted condition (0.0003 ± 0.0001, 0.0003 ± 0.00001, and 0.0003 ± 0.0001 mmol : mol in the DIP, DOP, and control treatments, respectively; Fig. 2a; Table 2).

Upon Fe-recovery, *Trichodesmium* decreased their Co : C ratio in the DOP treatment upon Fe-recovery (Fig. 3i); no significant differences were observed between mean steady-state Co : C ratio in the DIP and control treatments, while both of the latter were significantly higher than in the DOP treatment (0.0004 ± 0.0002, 0.0002 ± 0.0001, and 0.0003 ± 0.0001 mmol : mol in the DIP, DOP, and control treatments, respectively; Figs. 2a, 3i; Table 2). We do not have an explanation for why P-limitation would reduce *Trichodesmium* Co demand and this therefore warrants further studies to comprehensively understand biochemical processes involving Co in *Trichodesmium*.

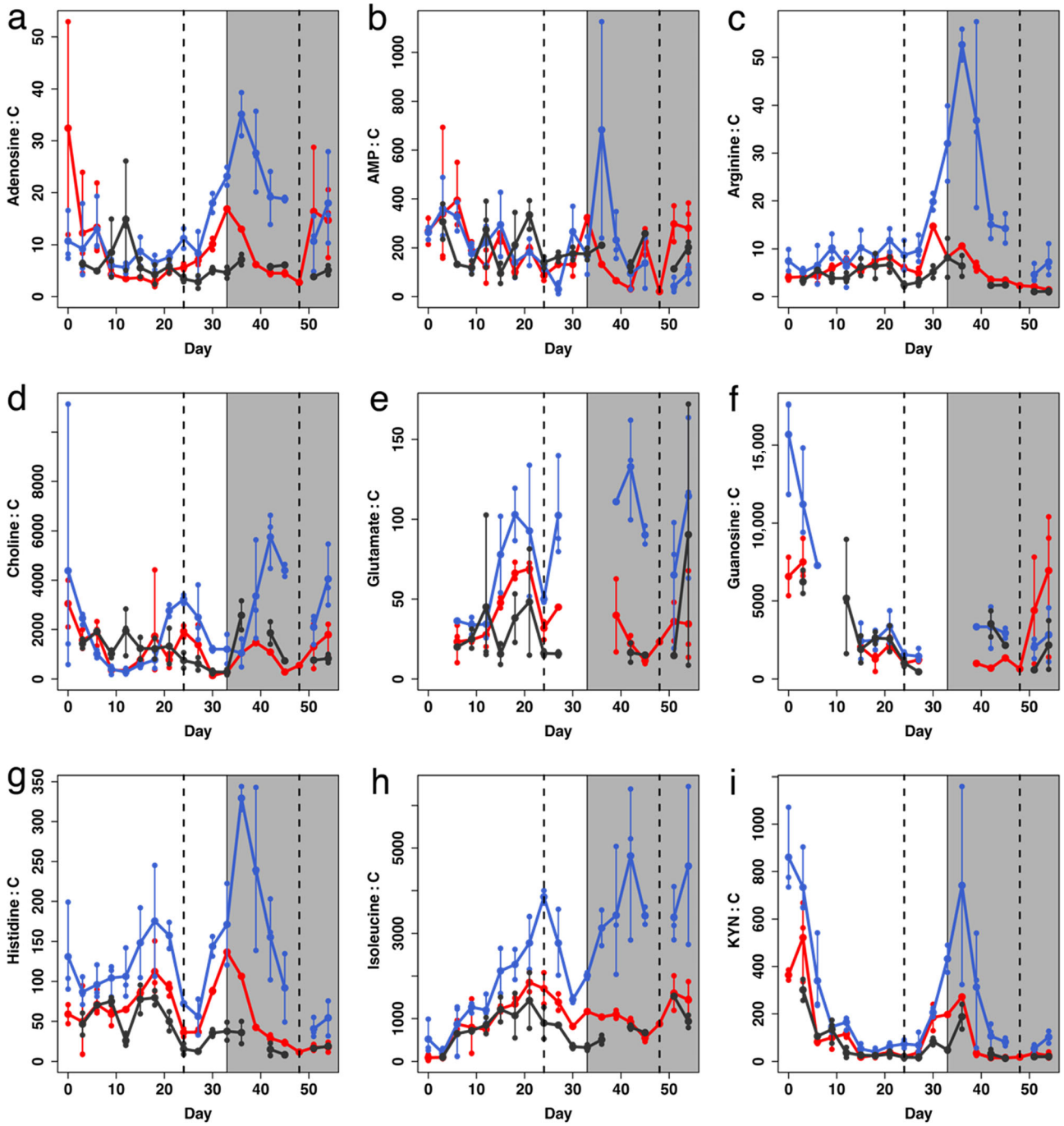

Fig 4. Particulate metabolite responses in *Trichodesmium* ISM101 for DIP and DOP treatments to different Fe supply concentrations. All metabolites are normalized to POC (μmol mol^{-1}). Points show triplicate measurements every 3 d, lines map the change in the mean value with time. The shaded region indicates where the high Fe (40 nM) media was introduced. The time period to the right side of the dashed line for each condition is considered here to be at steady state. KYN is short for Kynurenine, MTAP is short for *S*-methyl-5′-thioadenosine phosphorylase.

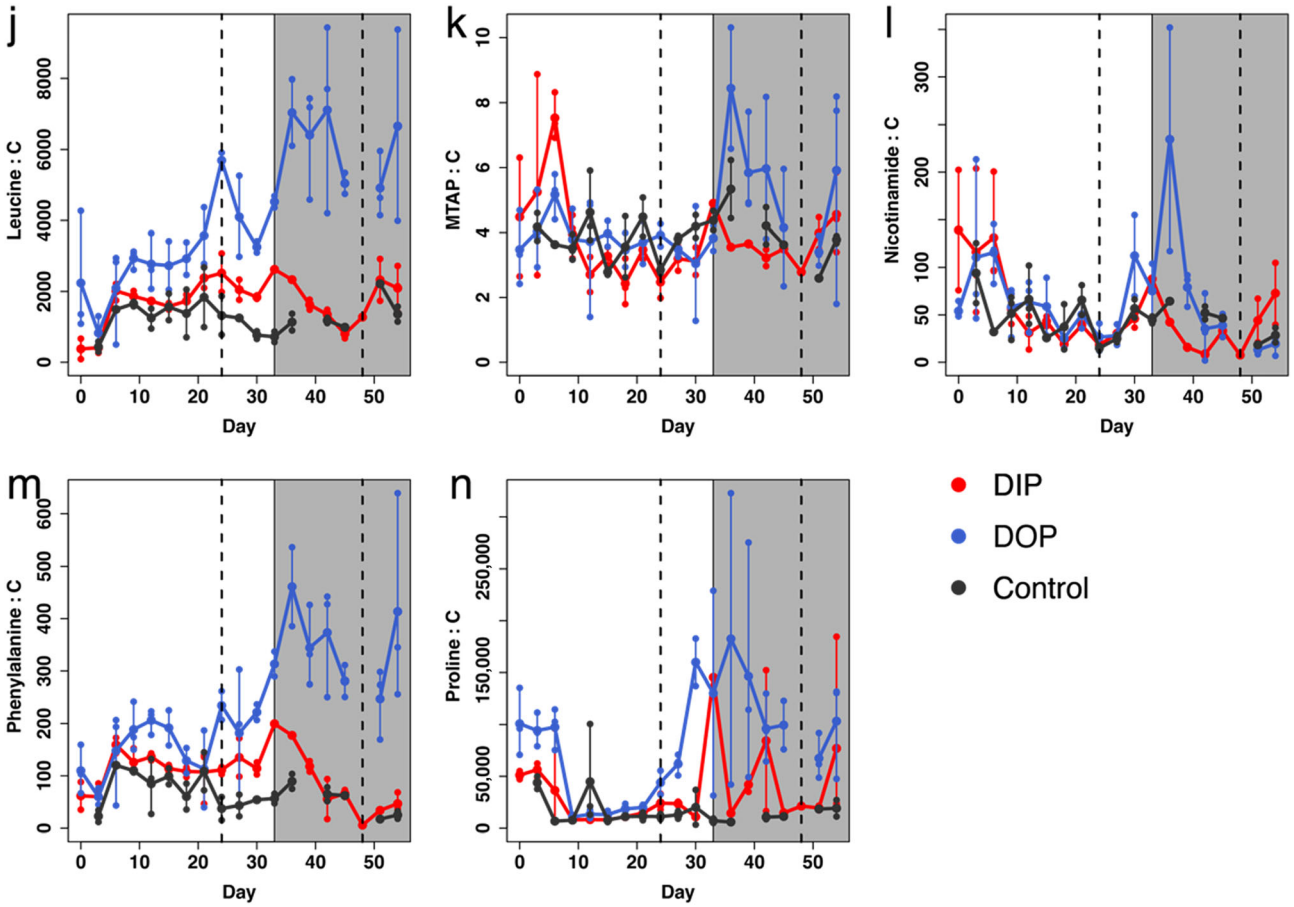

Fig 4 (Continued)

Particulate metabolites

Adenosine is a purine nucleoside serving as a building block for adenosine triphosphate, and its levels increase when adenosine triphosphate is metabolized when energy demands increase (Kujawinski et al. 2017). The adenosine : C in the DOP treatment increased by 1.34-fold compared to initial values under the Fe-depleted condition, this might indicate *Trichodesmium* under Fe–limitation condition requires more energy to support the acquisition of Fe. The adenosine : C in DIP treatment showed a decreasing and increasing trend under the Fe-depleted condition, with no significant differences detected between the mean steady-state adenosine : C in DIP and DOP treatments, while both of them were significantly higher than in the control treatment (Fig. 4). Upon initiation of the Fe recovery phase, adenosine : C continued to increase 1.5-fold in the DOP treatment over the first 3 d (days 33–36). We hypothesize that this reflects a continued strengthening of Fe-limitation in the DOP treatment, as shown by decreases in F_v/F_m over this time period and despite initiation of supply of the high Fe media (Schrader et al. 2011). Following this time lag, adenosine : C ratio in both of the DIP and DOP treatments decreased, while the mean steady-state adenosine : C ratio was still significantly higher than that in the control treatment (13 ± 10, 14 ± 8, and 5 ± 10 μmol mol^{-1} in the DIP, DOP, and control treatments, respectively).

Variations in the biomass-normalized abundances of some amino acids were also detected (Fig. 4). Under the Fe-depleted condition, significantly increased abundances of arginine, glutamate, histidine, isoleucine, leucine, phenylalanine, and proline were detected in both the DIP and DOP treatments, with abundances in the DOP treatment always significantly higher than those in DIP treatments. As for adenosine, the initial portion of the Fe-recovery phase for the DOP treatment was characterized by further increases in amino acids, potentially related to continued strengthening of Fe-limitation in this treatment as several Fe stress proteins (Fe starvation-induced protein A [IsiA and IsiB]) have been confirmed to be enriched in Fe-limited *Trichodesmium* (Chappell and Webb 2010; Snow et al. 2015; Walworth et al. 2016). Following this time lag, amino acids decreased or remained stable, with abundances always remaining higher for the DOP than for the DIP

treatment, which were statistically indistinguishable from the control treatment. The fixed N in *Trichodesmium* is assimilated via the glutamine synthetase–glutamate synthase pathway. In the 1st step, glutamine synthetase catalyzes the adenosine triphosphate–dependent condensation of glutamate with ammonium to glutamine (Liaw et al. 1995). Since Fe deficiency can limit N_2 fixation rates (Shi et al. 2007; Snow et al. 2015), *Trichodesmium* in Fe-depleted conditions may lead to a reduction in the amount of ammonium involved in glutamine synthesis due to the limitation of N_2 fixation by Fe-depletion, resulting in the accumulation of glutamate. Furthermore, glutamate is considered the primary precursor amino acid for proline synthesis, so the accumulation of glutamate may be the reason for the accumulation of the amount of proline (Verslues and Sharma 2010). The increase in the abundance of leucine and isoleucine was likely due to an increase in the abundance of pyruvate and threonine in *Trichodesmium*.

To compare changes in metabolite production by *Trichodesmium* in response to different nutrient concentrations and different P sources, we projected the carbon-normalized abundance of targeted metabolites into a lower-dimensional space using non-metric dimensional scaling (Supporting Information Fig. S4). Surprisingly, there were no significant changes in the carbon-normalized abundance of targeted metabolites produced by *Trichodesmium*, whether in the Fe-depleted, Fe-replete condition or transition phase from Fe-depleted to Fe-replete condition. Three possible reasons might be that (i) the changes in the abundance of proteins of *Trichodesmium* brought by Fe-limitation may not account for a significant amount of the proteome, resulting in insignificant changes in abundance of metabolites, for example, a recent study indicated the proteins that were upregulated under N- or P-limitation of *Emiliania huxleyi* accounted for only 1.7% and 5.7% of the total spectral counts, respectively (McKew et al. 2015); (ii) it is possible that during the pre-culturing phase prior to the start of the experiment, the growth of *Trichodesmium* had already induced changes in metabolites, such as *Trichodesmium* of the DOP treatment was under P-limitation at the start of the experiment, under conditions of phosphorus limitation a discernible reduction in adenosine 5′-monophosphate within diatoms has previously been found, concurrent with a concomitant elevation in adenosine (Kujawinski et al. 2017); (iii) the concentrations of metabolites exhibited large fluctuations even during the steady state, suggesting that the steady state of metabolites does not entirely coincide with that of *Trichodesmium* biomass.

Conclusions

We determined the elemental stoichiometry in *Trichodesmium* ISM101 under different Fe levels while supplying different P sources. Under conditions of Fe depletion, utilizing an exponentially fed batch culture system with a consistent culture dilution rate of 0.1 d^{-1}, we found a substantial reduction in carbon biomass within the DIP and DOP treatments, suggesting growth was limited by Fe-availability. When DIP was the supplied P source, reduced Fe supply resulted in increased Zn : C, Mn : C, Cu : C, and Mo : C ratios and a decreased Fe : C ratio. Conversely, when MPA was the supplied P source, reduced Fe supply resulted in an increased Zn : C ratio and decreased Fe : C, P : C, and N : C ratios. These results suggest *Trichodesmium* employs different strategies to cope with Fe-limitation, which is reflected in its elemental stoichiometry. Therefore, in the open ocean, *Trichodesmium* under Fe-limitation may increase its demand for Zn, Mn, and Mo, whereas *Trichodesmium* under Fe–P co-limitation may increase its demand for Zn. Concentrations of most nutrient-type metals in the surface waters are very low, and for example Zn concentrations follow a nutrient-like distribution, with low (pico- to nanomolar) concentrations in the surface ocean (Bruland and Lohan 2003; Middag et al. 2019). *Trichodesmium* may increase the demand for various metals in the surface ocean, thereby causing them to reach a depleted condition as increasing N inputs could drive a shift toward more widespread and stronger P stress (Moore et al. 2013) with surface waters are often approaching nutrient co-limitation (Browning and Moore 2023).

No significant changes were observed in the carbon-normalized abundance of targeted metabolites produced by *Trichodesmium*, whether in the Fe-depleted, Fe-replete condition or transition phase from Fe-depleted to Fe-replete condition. A possible reason for the lack of significant differences in the metabolome is that the changes in the abundance of proteins of *Trichodesmium* brought about by Fe-limitation may not account for a significant amount of the total proteome, resulting in insignificant changes in abundance of metabolites. Overall, these results are important for our understanding of how *Trichodesmium* respond to nutrient limitation and the feedback of the limitation on dissolved seawater nutrient distributions.

Conflict of Interest

The authors declare no conflicts of interest.

Data availability statement

Data have been deposited at Figshare (10.6084/m9.figshare.26148568).

References

Al-Hashem, A. A., A. J. Beck, S. Krisch, J.-L. Menzel Barraqueta, T. Steffens, and E. P. Achterberg. 2022. Particulate trace metal sources, cycling, and distributions on the Southwest African shelf. Glob. Biogeochem. Cycles **36**: e2022GB007453. doi:10.1029/2022GB007453

Ammerman, J. W. 1993. Microbial cycling of inorganic and organic phosphorus in the water column, p. 649–660. *In* Handbook of methods in aquatic microbial ecology. CRC Press.

Barofsky, A., C. Vidoudez, and G. Pohnert. 2009. Metabolic profiling reveals growth stage variability in diatom exudates. Limnol. Oceanogr. Methods **7**: 382–390. doi:10.4319/lom.2009.7.382

Barofsky, A., P. Simonelli, C. Vidoudez, C. Troedsson, J. C. Nejstgaard, H. H. Jakobsen, and G. Pohnert. 2010. Growth phase of the diatom *Skeletonema marinoi* influences the metabolic profile of the cells and the selective feeding of the copepod *Calanus* spp. J. Plankton Res. **32**: 263–272. doi:10.1093/plankt/fbp121

Becker, S., M. Aoyama, E. M. S. Woodward, K. Bakker, S. Coverly, C. Mahaffey, and T. Tanhua. 2020. GO-SHIP repeat hydrography nutrient manual: The precise and accurate determination of dissolved inorganic nutrients in seawater, using continuous flow analysis methods. Front. Mar. Sci. **7**: 581790.

Behrenfeld, M. J., and A. J. Milligan. 2013. Photophysiological expressions of iron stress in phytoplankton. Annu. Rev. Mar. Sci. **5**: 217–246. doi:10.1146/annurev-marine-121211-172356

Berman-Frank, I., A. Quigg, Z. V. Finkel, A. J. Irwin, and L. Haramaty. 2007. Nitrogen-fixation strategies and Fe requirements in cyanobacteria. Limnol. Oceanogr. **52**: 2260–2269. doi:10.4319/lo.2007.52.5.2260

Beversdorf, L. J., A. E. White, K. M. Björkman, R. M. Letelier, and D. M. Karl. 2010. Phosphonate metabolism by *Trichodesmium* IMS101 and the production of greenhouse gases. Limnol. Oceanogr. **55**: 1768–1778. doi:10.4319/lo.2010.55.4.1768

Browning, T. J., and C. M. Moore. 2023. Global analysis of ocean phytoplankton nutrient limitation reveals high prevalence of co-limitation. Nat. Commun. **14**: 5014. doi:10.1038/s41467-023-40774-0

Bruland, K. W., and M. C. Lohan. 2003. Controls of trace metals in seawater. Treatise Geochem. **6**: 625. doi:10.1016/B0-08-043751-6/06105-3

Capone, D. G., J. P. Zehr, H. W. Paerl, B. Bergman, and E. J. Carpenter. 1997. *Trichodesmium*, a globally significant marine cyanobacterium. Science **276**: 1221–1229. doi:10.1126/science.276.5316.1221

Carpenter, E. J., and D. G. Capone. 2008. Nitrogen Fixation in the Marine Environment. *In* Nitrogen in the marine environment. Elsevier.

Cerdan-Garcia, E., and others. 2021. Transcriptional responses of *Trichodesmium* to natural inverse gradients of Fe and P availability. ISME J **16**: 1055–1064. doi:10.1038/s41396-021-01151-1

Chappell, P. D., and E. A. Webb. 2010. A molecular assessment of the iron stress response in the two phylogenetic clades of *Trichodesmium*. Environ. Microbiol. **12**: 13–27. doi:10.1111/j.1462-2920.2009.02026.x

Chen, C.-C., I. B. Rodriguez, Y. L. Chen, J. P. Zehr, Y.-R. Chen, S.-T. D. Hsu, S.-C. Yang, and T.-Y. Ho. 2022. Nickel superoxide dismutase protects nitrogen fixation in *Trichodesmium*. Limnol. Oceanogr. Lett. **7**: 363–371. doi:10.1002/lol2.10263

Chen, Y. B., J. P. Zehr, and M. Mellon. 1996. Growth and nitrogen fixation of the diazotrophic filamentous nonheterocystous cyanobacterium *Trichodesmium* sp. IMS 101 in defined media: Evidence for a circadian rhythm. J. Phycol. **32**: 916–923. doi:10.1111/j.0022-3646.1996.00916.x

Clark, L. L., E. D. Ingall, and R. Benner. 1999. Marine organic phosphorus cycling; novel insights from nuclear magnetic resonance. Am. J. Sci. **299**: 724–737. doi:10.2475/ajs.299.7-9.724

Dawson, H. M., K. R. Heal, A. K. Boysen, L. T. Carlson, A. E. Ingalls, and J. N. Young. 2020. Potential of temperature- and salinity-driven shifts in diatom compatible solute concentrations to impact biogeochemical cycling within sea ice. Elementa **8**: 25. doi:10.1525/elementa.421

Dominic, B., S. Zani, Y. Chen, M. T. Mellon, and J. P. Zehr. 2000. Organization of the nif genes of the nonheterocystous cyanobacterium *Trichodesmium* sp. IMS101. J. Phycol. **36**: 693–701. doi:10.1046/j.1529-8817.2000.99208.x

Duhamel, S., S. T. Dyhrman, and D. M. Karl. 2010. Alkaline phosphatase activity and regulation in the North Pacific Subtropical Gyre. Limnol. Oceanogr. **55**: 1414–1425. doi:10.4319/lo.2010.55.3.1414

Durham, B. P., S. P. Dearth, S. Sharma, S. A. Amin, C. B. Smith, S. R. Campagna, E. V. Armbrust, and M. A. Moran. 2017. Recognition cascade and metabolite transfer in a marine bacteria-phytoplankton model system. Environ. Microbiol. **19**: 3500–3513. doi:10.1111/1462-2920.13834

Dyhrman, S. T., P. D. Chappell, S. T. Haley, J. W. Moffett, E. D. Orchard, J. B. Waterbury, and E. A. Webb. 2006. Phosphonate utilization by the globally important marine diazotroph *Trichodesmium*. Nature **439**: 68–71. doi:10.1038/nature04203

Falkowski, P. G. 1997. Evolution of the nitrogen cycle and its influence on the biological sequestration of CO_2 in the ocean. Nature **387**: 272–275. doi:10.1038/387272a0

Fiore, C. L., K. Longnecker, M. C. Kido Soule, and E. B. Kujawinski. 2015. Release of ecologically relevant metabolites by the cyanobacterium *Synechococcus elongatus* CCMP 1631. Environ. Microbiol. **17**: 3949–3963. doi:10.1111/1462-2920.12899

Fischer, R., T. Andersen, H. Hillebrand, and R. Ptacnik. 2014. The exponentially fed batch culture as a reliable alternative to conventional chemostats. Limnol. Oceanogr. Methods **12**: 432–440. doi:10.4319/lom.2014.12.432

Frischkorn, K. R., S. T. Haley, and S. T. Dyhrman. 2019. Transcriptional and proteomic choreography under phosphorus deficiency and re-supply in the N2 fixing cyanobacterium *Trichodesmium erythraeum*. Front. Microbiol. **10**: 1–13. doi:10.3389/fmicb.2019.00330

Garcia, N. S., F. Fu, P. N. Sedwick, and D. A. Hutchins. 2015. Iron deficiency increases growth and nitrogen-fixation rates of phosphorus-deficient marine cyanobacteria. ISME J. **9**: 238–245. doi:10.1038/ismej.2014.104

Heal, K. R., N. A. Kellogg, L. T. Carlson, R. M. Lionheart, and A. E. Ingalls. 2019. Metabolic consequences of cobalamin scarcity in the diatom *Thalassiosira pseudonana* as revealed through metabolomics. Protist **170**: 328–348. doi:10.1016/j.protis.2019.05.004

Held, N. A., and others. 2020. Co-occurrence of Fe and P stress in natural populations of the marine diazotroph *Trichodesmium*. Biogeosciences **17**: 2537–2551. doi:10.5194/bg-17-2537-2020

Hernandez, J. A., S. J. George, and L. M. Rubio. 2009. Molybdenum trafficking for nitrogen fixation. Biochemistry **48**: 9711–9721. doi:10.1021/bi901217p

Ho, T.-Y. 2013. Nickel limitation of nitrogen fixation in *Trichodesmium*. Limnol. Oceanogr. **58**: 112–120. doi:10.4319/lo.2013.58.1.0112

Ho, T. Y., A. Quigg, Z. V. Finkel, A. J. Milligan, K. Wyman, P. G. Falkowski, and F. M. M. Morel. 2003. The elemental composition of some marine phytoplankton. J. Phycol. **39**: 1145–1159. doi:10.1111/j.0022-3646.2003.03-090.x

Ho, T. Y., T. H. Chu, and C. L. Hu. 2013. Interrelated influence of light and Ni on *Trichodesmium* growth. Front. Microbiol. **4**: 1–6. doi:10.3389/fmicb.2013.00139

Honey, D., M. Gledhill, T. Bibby, F. Legiret, N. Pratt, A. Hickman, T. Lawson, and E. Achterberg. 2013. Heme b in marine phytoplankton and particulate material from the North Atlantic Ocean. Mar. Ecol. Prog. Ser. **483**: 1–17. doi:10.3354/meps10367

Hynes, A. M., P. D. Chappell, S. T. Dyhrman, S. C. Doney, and E. A. Webb. 2009. Cross-basin comparison of phosphorus stress and nitrogen fixation in *Trichodesmium*. Limnol. Oceanogr. **54**: 1438–1448. doi:10.4319/lo.2009.54.5.1438

Ji, Y., and R. M. Sherrell. 2008. Differential effects of phosphorus limitation on cellular metals in *Chlorella* and *Microcystis*. Limnol. Oceanogr. **53**: 1790–1804. doi:10.4319/lo.2008.53.5.1790

Johnson, W. M., M. C. Kido Soule, and E. B. Kujawinski. 2016. Evidence for quorum sensing and differential metabolite production by a marine bacterium in response to DMSP. ISME J. **10**: 2304–2316. doi:10.1038/ismej.2016.6

Johnson, W. M., M. C. Kido Soule, K. Longnecker, M. P. Bhatia, S. J. Hallam, M. W. Lomas, and E. B. Kujawinski. 2023. Particulate and dissolved metabolite distributions along a latitudinal transect of the western Atlantic Ocean. Limnol. Oceanogr. **68**: 377–393.

Kaushik, M. S., M. Srivastava, E. Verma, and A. K. Mishra. 2015. Role of manganese in protection against oxidative stress under iron starvation in cyanobacterium *Anabaena* 7120. J. Basic Microbiol. **55**: 729–740. doi:10.1002/jobm.201400742

Kido Soule, M. C., K. Longnecker, W. M. Johnson, and E. B. Kujawinski. 2015. Environmental metabolomics: Analytical strategies. Mar. Chem. **177**: 374–387. doi:10.1016/j.marchem.2015.06.029

Kim, E. E., and H. W. Wyckoff. 1991. Reaction mechanism of alkaline phosphatase based on crystal structures. J. Mol. Biol. **218**: 449–464.

Kujawinski, E. B., K. Longnecker, H. Alexander, S. T. Dyhrman, C. L. Fiore, S. T. Haley, and W. M. Johnson. 2017. Phosphorus availability regulates intracellular nucleotides in marine eukaryotic phytoplankton. Limnol. Oceanogr. Lett. **2**: 119–129. doi:10.1002/lol2.10043

Kustka, A. B., S. A. Sañudo-Wilhelmy, E. J. Carpenter, D. Capone, J. Burns, and W. G. Sunda. 2004. Iron requirements for dinitrogen- and ammonium-supported growth in cultures of *Trichodesmium* (IMS 101): Comparison with nitrogen fixation rates and iron : carbon ratios of field populations. Limnol. Oceanogr. **49**: 1224. doi:10.4319/lo.2004.49.4.1224

Liaw, S.-H., I. Kuo, and D. Eisenberg. 1995. Discovery of the ammonium substrate site on glutamine synthetase, a third cation binding site. Protein Sci. **4**: 2358–2365. doi:10.1002/pro.5560041114

Luo, H., H. Zhang, R. A. Long, and R. Benner. 2011. Depth distributions of alkaline phosphatase and phosphonate utilization genes in the North Pacific Subtropical Gyre. Aquat. Microb. Ecol. **62**: 61–69. doi:10.3354/ame01458

Mahaffey, C., S. Reynolds, C. E. Davis, and M. C. Lohan. 2014. Alkaline phosphatase activity in the subtropical ocean: Insights from nutrient, dust and trace metal addition experiments. Front. Mar. Sci. **1**: 1–13. doi:10.3389/fmars.2014.00073

Mark Moore, C., and others. 2009. Large-scale distribution of Atlantic nitrogen fixation controlled by iron availability. Nat. Geosci. **2**: 867–871. doi:10.1038/ngeo667

Marki, A., R. Fischer, T. J. Browning, E. Louropoulou, R. Ptacnik, and M. Gledhill. 2020. Stoichiometry of Fe, Mn and Co in the marine diazotroph *Crocosphaera subtropica* ATCC51142 in Fe- and P-limited continuous cultures. Mar. Ecol. Prog. Ser. **656**: 19–33. doi:10.3354/meps13523

Mausz, M. A., and G. Pohnert. 2015. Phenotypic diversity of diploid and haploid *Emiliania huxleyi* cells and of cells in different growth phases revealed by comparative metabolomics. J. Plant Physiol. **172**: 137–148. doi:10.1016/j.jplph.2014.05.014

McKew, B. A., G. Metodieva, C. A. Raines, M. V. Metodiev, and R. J. Geider. 2015. Acclimation of *Emiliania huxleyi* (1516) to nutrient limitation involves precise modification of the proteome to scavenge alternative sources of N and P. Environ. Microbiol. **17**: 4050–4062. doi:10.1111/1462-2920.12957

Metcalf, W. W., and others. 2012. Synthesis of methylphosphonic acid by marine microbes: A source for methane in the aerobic ocean. Science **337**: 1104–1107. doi:10.1126/science.1219875

Middag, R., H. J. W. de Baar, and K. W. Bruland. 2019. The relationships between dissolved zinc and major nutrients phosphate and silicate along the GEOTRACES GA02 transect in the west Atlantic Ocean. Glob. Biogeochem. Cycles **33**: 63–84. doi:10.1029/2018GB006034

Moore, C. M., and others. 2013. Processes and patterns of oceanic nutrient limitation. Nat. Geosci. **6**: 701–710. doi:10.1038/ngeo1765

Morrissey, J., and C. Bowler. 2012. Iron utilization in marine cyanobacteria and eukaryotic algae. Front. Microbiol. **3**: 1–13. doi:10.3389/fmicb.2012.00043

Nuester, J., S. Vogt, M. Newville, A. B. Kustka, and B. S. Twining. 2012. The unique biogeochemical signature of the marine diazotroph *Trichodesmium*. Front. Microbiol. **3**: 1–15. doi:10.3389/fmicb.2012.00150

Orchard, E. D., J. W. Ammerman, M. W. Lomas, and S. T. Dyhrman. 2010. Dissolved inorganic and organic phosphorus uptake in *Trichodesmium* and the microbial community: The importance of phosphorus ester in the Sargasso Sea. Limnol. Oceanogr. **55**: 1390–1399. doi:10.4319/lo.2010.55.3.1390

Palenik, B., and F. M. M. Morel. 1991. Amine oxidases of marine phytoplankton. Appl. Environ. Microbiol. **57**: 2440–2443. doi:10.1128/aem.57.8.2440-2443.1991

Pau, R. N. 2004. Molybdenum uptake and homeostasis, p. 225–256. *In* Genetics and regulation of nitrogen fixation in free-living bacteria. Springer.

Peers, G., and N. M. Price. 2004. A role for manganese in superoxide dismutases and growth of iron-deficient diatoms. Limnol. Oceanogr. **49**: 1774–1783. doi:10.4319/lo.2004.49.5.1774

Peers, G., S. A. Quesnel, and N. M. Price. 2005. Copper requirements for iron acquisition and growth of coastal and oceanic diatoms. Limnol. Oceanogr. **50**: 1149–1158. doi:10.4319/lo.2005.50.4.1149

Peers, G., and N. M. Price. 2006. Copper-containing plastocyanin used for electron transport by an oceanic diatom. Nature **441**: 341–344. doi:10.1038/nature04630

Puppo, A., and J. Rigaud. 1986. Superoxide dismutase: An essential role in the protection of the nitrogen fixation process? FEBS Lett. **201**: 187–189. doi:10.1016/0014-5793(86)80605-6

Raven, J. A., M. C. W. Evans, and R. E. Korb. 1999. The role of trace metals in photosynthetic electron transport in O_2-evolving organisms. Photosynth. Res. **60**: 111–150. doi:10.1023/a:1006282714942

Rodriguez, F., J. Lillington, S. Johnson, C. R. Timmel, S. M. Lea, and B. C. Berks. 2014. Crystal structure of the *Bacillus subtilis* phosphodiesterase PhoD reveals an iron and calcium-containing active site. J. Biol. Chem. **289**: 30889–30899. doi:10.1074/jbc.M114.604892

Salomon, E., and N. Keren. 2011. Manganese limitation induces changes in the activity and in the organization of photosynthetic complexes in the cyanobacterium *Synechocystis* sp. strain PCC 6803. Plant Physiol. **155**: 571–579. doi:10.1104/pp.110.164269

Salomon, E., and N. Keren. 2015. Acclimation to environmentally relevant Mn concentrations rescues a cyanobacterium from the detrimental effects of iron limitation. Environ. Microbiol. **17**: 2090–2098. doi:10.1111/1462-2920.12826

Sannigrahi, P., E. D. Ingall, and R. Benner. 2006. Nature and dynamics of phosphorus-containing components of marine dissolved and particulate organic matter. Geochim. Cosmochim. Acta **70**: 5868–5882. doi:10.1016/j.gca.2006.08.037

Schoffman, H., H. Lis, Y. Shaked, and N. Keren. 2016. Iron–nutrient interactions within phytoplankton. Front. Plant Sci. **7**: 1–12. doi:10.3389/fpls.2016.01223

Schrader, P. S., A. J. Milligan, and M. J. Behrenfeld. 2011. Surplus photosynthetic antennae complexes underlie diagnostics of iron limitation in a cyanobacterium. PLoS One **6**: e18753. doi:10.1371/journal.pone.0018753

Shao, Z., and others. 2023. Global oceanic diazotroph database version 2 and elevated estimate of global oceanic N_2 fixation. Earth Syst. Sci. Data **15**: 3673–3709. doi:10.5194/essd-15-3673-2023

Sharon, S., and others. 2014. The hierarchy of transition metal homeostasis: Iron controls manganese accumulation in a unicellular cyanobacterium. Biochim. Biophys. Acta Bioenerg. **1837**: 1990–1997. doi:10.1016/j.bbabio.2014.09.007

Shi, T., Y. Sun, and P. G. Falkowski. 2007. Effects of iron limitation on the expression of metabolic genes in the marine cyanobacterium *Trichodesmium erythraeum* IMS101. Environ. Microbiol. **9**: 2945–2956. doi:10.1111/j.1462-2920.2007.01406.x

Shi, D., S. A. Kranz, J. M. Kim, and F. M. M. Morel. 2012. Ocean acidification slows nitrogen fixation and growth in the dominant diazotroph *Trichodesmium* under low-iron conditions. Proc. Natl. Acad. Sci. USA **109**: E3094–E3100. doi:10.1073/pnas.1216012109

Snow, J. T., D. Polyviou, P. Skipp, N. A. M. Chrismas, A. Hitchcock, R. Geider, C. M. Moore, and T. S. Bibby. 2015. Quantifying integrated proteomic responses to iron stress in the globally important marine diazotroph *Trichodesmium*. PLoS One **10**: 1–24. doi:10.1371/journal.pone.0142626

Sohm, J. A., E. A. Webb, and D. G. Capone. 2011. Emerging patterns of marine nitrogen fixation. Nat. Rev. Microbiol. **9**: 499–508. doi:10.1038/nrmicro2594

Stosiek, N., M. Talma, and M. Klimek-Ochab. 2020. Carbon–phosphorus lyase—the state of the art. Appl. Biochem. Biotechnol. **190**: 1525–1552. doi:10.1007/s12010-019-03161-4

Suggett, D. J., C. M. Moore, A. E. Hickman, and R. J. Geider. 2009. Interpretation of fast repetition rate (FRR) fluorescence: Signatures of phytoplankton community structure versus physiological state. Mar. Ecol. Prog. Ser. **376**: 1–19. doi:10.3354/meps07830

Trimborn, S., S. Thoms, T. Brenneis, J. P. Heiden, S. Beszteri, and K. Bischof. 2017. Two Southern Ocean

diatoms are more sensitive to ocean acidification and changes in irradiance than the prymnesiophyte *Phaeocystis antarctica*. Physiol. Plant. **160**: 155–170. doi:10.1111/ppl.12539

Tuit, C., J. Waterbury, and G. Ravizza. 2004. Diel variation of molybdenum and iron in marine diazotrophic cyanobacteria. Limnol. Oceanogr. **49**: 978–990. doi:10.4319/lo.2004.49.4.0978

Tuo, S.-H., I. B. Rodriguez, and T. Y. Ho. 2020. H2 accumulation and N_2 fixation variation by Ni limitation in Cyanothece. Limnol. Oceanogr. **65**: 377–386. doi:10.1002/lno.11305

Twining, B. S., D. Nuñez-Milland, S. Vogt, R. S. Johnson, and P. N. Sedwick. 2010. Variations in *Synechococcus* cell quotas of phosphorus, sulfur, manganese, iron, nickel, and zinc within mesoscale eddies in the Sargasso Sea. Limnol. Oceanogr. **55**: 492–506. doi:10.4319/lo.2009.55.2.0492

Tzubari, Y., L. Magnezi, A. Be'er, and I. Berman-Frank. 2018. Iron and phosphorus deprivation induce sociality in the marine bloom-forming cyanobacterium *Trichodesmium*. ISME J. **12**: 1682–1693. doi:10.1038/s41396-018-0073-5

van de Poll, W. H., E. Abdullah, R. J. W. Visser, P. Fischer, and A. G. J. Buma. 2020. Taxon-specific dark survival of diatoms and flagellates affects Arctic phytoplankton composition during the polar night and early spring. Limnol. Oceanogr. **65**: 903–914. doi:10.1002/lno.11355

Verslues, P. E., and S. Sharma. 2010. Proline metabolism and its implications for plant–environment interaction. Arabidopsis Book **8**: e0140. doi:10.1199/tab.0140

Vidoudez, C., and G. Pohnert. 2012. Comparative metabolomics of the diatom *Skeletonema marinoi* in different growth phases. Metabolomics **8**: 654–669. doi:10.1007/s11306-011-0356-6

Walworth, N. G., F. X. Fu, E. A. Webb, M. A. Saito, D. Moran, M. R. McLlvin, M. D. Lee, and D. A. Hutchins. 2016. Mechanisms of increased *Trichodesmium* fitness under iron and phosphorus co-limitation in the present and future ocean. Nat. Commun. **7**: 1–11. doi:10.1038/ncomms12081

Walworth, N. G., F. X. Fu, M. D. Lee, X. Cai, M. A. Saito, E. A. Webb, and D. A. Hutchins. 2018. Nutrient-colimited *Trichodesmium* as a nitrogen source or sink in a future ocean. Appl. Environ. Microbiol. **84**: 1–14. doi:10.1128/AEM.02137-17

Wang, X., T. J. Browning, E. P. Achterberg, and M. Gledhill. 2022. Phosphorus limitation enhances diazotroph zinc quotas. Front. Microbiol. **13**: 1–9. doi:10.3389/fmicb.2022.853519

White, A. E., Y. H. Spitz, D. M. Karl, and R. M. Letelier. 2006. Flexible elemental stoichiometry in *Trichodesmium* spp. and its ecological implications. Limnol. Oceanogr. **51**: 1777–1790. doi:10.4319/lo.2006.51.4.1777

Wu, Z., B. Zeng, R. Li, and L. Song. 2012. Physiological regulation of *Cylindrospermopsis raciborskii* (Nostocales, Cyanobacteria) in response to inorganic phosphorus limitation. Harmful Algae **15**: 53–58. doi:10.1016/j.hal.2011.11.005

Yamaguchi, T., K. Furuya, M. Sato, and K. Takahashi. 2016. Phosphate release due to excess alkaline phosphatase activity in *Trichodesmium erythraeum*. Plankton Benthos Res. **11**: 29–36. doi:10.3800/pbr.11.29

Yong, S. C., and others. 2014. A complex iron-calcium cofactor catalyzing phosphotransfer chemistry. Science **345**: 1170–1173. doi:10.1126/science.1254237

Zehr, J. P., and D. G. Capone. 2020. Changing perspectives in marine nitrogen fixation. Science **368**: eaay9514. doi:10.1126/science.aay9514

Acknowledgments

We thank T. Steffens, A. Mutzberg, D. Jasinski, and K. Nachtigall for technical assistance. X. Wang is grateful to the China Scholarship Council (CSC) for providing financial support (File No. 201706330098). Open Access funding enabled and organized by Projekt DEAL.

Submitted 25 August 2023
Revised 29 March 2024
Accepted 29 September 2024

Associate editor: Takuhei Shiozaki